A&A 478, 83–92 (2008)
DOI: 10.1051/0004-6361:20078332

Astronomy & Astrophysics

The great observatories origins deep survey

VLT/FORS2 spectroscopy in the GOODS-South field: Part III⋆

E. Vanzella[1], S. Cristiani[1], M. Dickinson[2], M. Giavalisco[3], H. Kuntschner[4], J. Haase[4], M. Nonino[1], P. Rosati[5] C. Cesarsky[5], H. C. Ferguson[6], R. A. E. Fosbury[4], A. Grazian[7], L. A. Moustakas[8], A. Rettura[9], P. Popesso[5], A. Renzini[10], D. Stern[8], and the GOODS Team

[1] INAF – Astronomical Observatory of Trieste, via G.B. Tiepolo 11, 34143 Trieste, Italy
e-mail: vanzella@oats.inaf.it
[2] National Optical Astronomy Obs., PO Box 26732, Tucson, AZ 85726, USA
[3] University of Massachusetts, Department of Astronomy, Amherst, MA, 01003, USA
[4] ST-ECF, Karl-Schwarzschild Str. 2, 85748 Garching, Germany
[5] European Southern Observatory, Karl-Schwarzschild-Strasse 2, Garching 85748, Germany
[6] Space Telescope Science Institute, 3700 San Martin Drive, Baltimore, MD 21218, USA
[7] INAF – Osservatorio Astronomico di Roma, via Frascati 33, 00040 Monteporzio Roma, Italy
[8] Jet Propulsion Laboratory, California Institute of Technology, MS 169-506, 4800 Oak Grove Drive, Pasadena, CA 91109, USA
[9] Johns Hopkins University, 3400 N. Charles Street, Baltimore, MD, 21218, USA
[10] INAF – Astronomical Observatory of Padova, Vicolo dell'Osservatorio 5, 35122 Padova, Italy⋆⋆

Received 23 July 2007 / Accepted 22 October 2007

ABSTRACT

Aims. We present the full data set of the spectroscopic campaign of the ESO/GOODS program in the GOODS-South field, obtained with the FORS2 spectrograph at the ESO/VLT.
Methods. Objects were selected as candidates for VLT/FORS2 observations primarily based on the expectation that the detection and measurement of their spectral features would benefit from the high throughput and spectral resolution of FORS2. The reliability of the redshift estimates is assessed using the redshift-magnitude and color-redshift diagrams, and comparing the results with public data.
Results. Including the third part of the spectroscopic campaign (12 masks) to the previous work (26 masks, Vanzella et al. 2005, 2006), 1715 spectra of 1225 individual targets have been analyzed. The actual spectroscopic catalog provides 887 redshift determinations. The typical redshift uncertainty is estimated to be $\sigma_z \simeq 0.001$. Galaxies have been selected adopting different color criteria and using photometric redshifts. The resulting redshift distribution typically spans two domains: from $z = 0.5$ to 2 and $z = 3.5$ to 6.3. The reduced spectra and the derived redshifts are released to the community through the ESO web page http://www.eso.org/science/goods/.

Key words. cosmology: observations – cosmology: large scale – structure of the universe – galaxies: evolution

1. Introduction

The Great Observatories Origins Deep Survey (GOODS) is a public, multi-facility project started in the early 2000 designed to gather the best and deepest multiwavelength data for studying the formation and evolution of galaxies and active galactic nuclei, the distribution of dark and luminous matter at high redshift, the cosmological parameters from distant supernovae (Riess et al. 2004), and the extragalactic background light (for an overview of GOODS, see Dickinson et al. 2001, 2003; Renzini et al. 2003; Giavalisco et al. 2004a).

The program targets two carefully selected fields, the Hubble Deep Field North (HDF-N) and the Chandra Deep Field South (CDF-S), with three NASA Great Observatories (HST, Spitzer and Chandra), ESA's XMM-Newton, and a wide variety of ground-based facilities. The area common to all the observing programs is 320 arcmin^2, equally divided between the North and South fields. In the last five years the CDF-S has been the target of several spectroscopic campaigns (Cristiani et al. 2000; Croom et al. 2001; Bunker et al. 2003; Stanway et al. 2004; Strolger et al. 2004; van der Wel et al. 2004; Dickinson et al. 2004; Szokoly et al. 2004; Le Fevre et al. 2005; Mignoli et al. 2005; Ravikumar et al. 2007).

This is the third paper in a series presenting the results of the GOODS spectroscopic program carried out with the VLT/FORS2 spectrograph. For a full description of its aims we refer to the first two articles (Vanzella et al. 2005 – RUN1, 2006 – RUN2, V05 and V06, hereafter).

Here we recall that the ESO/GOODS spectroscopic program is designed to observe all galaxies for which VLT optical spectroscopy is likely to allow the redshift determination. The program makes full use of the VLT instrument capabilities (FORS2 and VIMOS), matching targets to instrument and disperser combinations in order to maximize the effectiveness of the observations. The magnitude limits and selection bandpasses

⋆ Table 1 is only available in electronic form at the CDS via anonymous ftp to cdsarc.u-strasbg.fr (130.79.128.5) or via http://cdsweb.u-strasbg.fr/cgi-bin/qcat?J/A+A/478/83

⋆⋆ Based on observations made at the European Southern Observatory, Paranal, Chile (ESO programme 170.A-0788 *The Great Observatories Origins Deep Survey: ESO Public Observations of the SIRTF Legacy/HST Treasury/Chandra Deep Field South*).

to some extent depend on the instrumental setup being used. In the present sample, the mean z_{850} magnitude at redshift below 2 is 23.16±1.20, while for the higher redshift part it is 25.34±0.84.

In the present paper we present the entire FORS2 spectroscopic campaign (including new 12 masks). Half of these 12 masks have been observed in visitor mode during December 2004 (RUN3, hereafter), and the other six masks (RUN4, hereafter) in the period 2005 – middle 2006 in service mode. Observations performed in December 2004 were mainly focused on color-selected Lyman break "dropout" targets and the last six masks (RUN4) were mainly dedicated to Lyman break "dropout" and sources detected at 24 μm with the Multiband Imaging Photometer for Spitzer (MIPS) instrument aboard the *Spitzer Space Telescope*. 180 new redshift measurements out of 345 individual sources have been derived from RUN3 and RUN4, several galaxies have been observed two or three times (mainly V_{606}-dropouts and i_{775}-dropouts) in order to gain signal, in this way 38 confirmation at redshift beyond 5 have been carried out.

The VIMOS spectroscopic survey in the GOODS-S field has completed its run and hundreds of redshift determinations will be released, mainly in the redshift range $0 < z \leq 3.5$ (Popesso et al. in preparation).

The paper is organized as follows. Section 2 describes the target selection, while Sect. 3 describes the observations and data reductions. The redshift determination is presented in Sect. 4. In Sect. 5 we discuss the full data set and in Sect. 6 we discuss two individual sources. In Sect. 7 we summarize briefly the whole spectroscopic campaign and give our conclusions.

Throughout this paper the magnitudes are given in the AB system[1] and the ACS *F435W*, *F606W*, *F775W*, and *F850LP* filters are designated hereafter as B_{435}, V_{606}, i_{775} and z_{850}, respectively. We assume a cosmology with $\Omega_{\rm tot}, \Omega_M, \Omega_\Lambda = 1.0, 0.3, 0.7$ and $H_0 = 70$ km s^{-1} Mpc^{-1}.

2. Target selection

The selection of galaxies have already been described in V05 and V06. Here we recall the adopted criteria:

1. Primary catalog: $(i_{775} - z_{850}) > 0.6$ and $z_{850} < 26$. This should ensure redshifts $z \gtrsim 0.7$ for ordinary early-type galaxies (whose strongest features are expected to be absorption lines), and higher redshifts for intrinsically bluer galaxies likely to have emission lines.
2. Secondary catalog: $0.45 < (i_{775} - z_{850}) < 0.6$ and $z_{850} < 26$.
3. Photometric-redshift sample: $1 < z_{\rm phot} < 2$ and $z_{850} < 26$, from Mobasher et al. (2004).
4. B_{435}, V_{606} and i_{775}-dropouts color selected Lyman break galaxy candidates (see Giavalisco et al. 2004b; and Dickinson et al. 2004). The B_{435}-dropouts sources have been selected adopting color criteria slightly different from Giavalisco et al. (2004b): $(B_{435} - V_{606}) > 1.1$, $(V_{606} - z_{850}) < 1.6$ and $(B_{435} - V_{606}) > (V_{606} - z_{850}) + 1.1$.
5. A few miscellaneous objects, including host galaxies of supernovae detected in the GOODS ACS observing campaign.

In the first RUN (V05), targets were selected from a preliminary catalog based on 3-epoch v0.5 GOODS ACS images.

In the following RUNs (2, 3 and 4), targets were selected from the ACS catalog version r1.1z, based on the 5-epoch v1.0 ACS images. The r1.1z catalog is drawn from the r1.0z SExtractor run, and merely corrects errors and omissions in the r1.0z catalog files. The majority of the targets have been selected following the above criteria, in particular giving priority to LBGs. Additionally, in RUN4, sources detected at 24 μm with the MIPS were included to fill out the masks. In addition to requiring 24 μm detection, these sources were selected on their optical properties to take advantage of the FORS2 red performance, and mainly consisted of MIPS-detected extremely red objects (EROs) and distant red galaxies (DRGs; see Papovich et al. 2006) with photometric redshift $z_{\rm phot} < 1.65$, thus putting them in a range where FORS2 may be capable of measuring redshifts.

For this data release, that includes the entire GOODS/FORS2 campaign (RUN1, 2, 3, 4) the objects have been matched to the ACS catalog version r1.1z.

1715 spectra of 1225 individual targets have been extracted from all RUNs (multiple observations have been carried out, especially for the high redshift candidates). The FORS2 spectroscopic catalog lists 887 redshift determinations in the GOODS-S field.

3. Observations and data reduction

The VLT/FORS2 spectroscopic observations were carried out in service and visitor (RUN3) mode between October of 2002 and October of 2006. A summary of the observations is presented in Table 2. Considering the previous works (V05, V06, 26 FORS2 masks) and the present work (RUN3 and RUN4, 12 masks), a total of 38 FORS2 masks have been acquired. In all cases the 300*I* grism was used as dispersing element without order-separating filter. This grism provides a scale of roughly 3.2 Å pix^{-1}. The nominal resolution of the configuration was $R = \lambda/\Delta\lambda = 660$, which corresponds to 13 Å at 8600 Å. The spatial scale of FORS2 is 0.126″/pixel. The slit width was always 1″. In order to effectively improve the sky and fringe subtraction and remove CCD blemishes, dithering of the targets along the slits was applied, with typically steps of 0, ±8 pixels during RUNs 1 and 2, and 0, ±6 pixels in RUNs 3 and 4. In general the spectral coverage ranges from 6000 to 10 000 Å.

3.1. Data reduction

Data have been reduced with a semi-automatic pipeline that we have developed on the basis of the MIDAS package (Warmels 1991), using commands of the LONG and MOS contexts. We have used the procedures described in the previous works (V05, V06) with minor improvements.

In the case of multiple observations of the same source in different masks, the one dimensional spectra have been co-added weighting according to the exposure time, the seeing condition and the resulting quality of each extraction process (defects present in the CCD, object too close to the end of the slit, etc.). A visual check of the two dimensional frames has been performed and in some cases the two dimensional spectra have also been co-added, in order to improve and guide the visual inspection.

We emphasize here that we opted to observe the science targets *without* an order-sorting filter, implying deleterious effects to the flux calibration. The second order overlap becomes important at wavelengths above ~8000 Å depending on the color of the target. However, the fluxes derived from spectra are in general consistent with the ACS photometry (an example for a red and blue source is shown in V06, Fig. 1).

[1] Oke (1977), $AB \equiv 31.4 - 2.5 \log\langle f_\nu/\mathrm{nJy}\rangle$.

Table 1. Spectroscopic redshift catalog†.

ID(v1.1)	z_{850}	$(i_{775} - z_{850})$	z spec	Class.	Quality	Comments
GDS J033245.99-275108.3	23.48	0.47	1.238	em.	B	[O II]3727
GDS J033246.04-274929.7	26.06	1.77	5.787	em.	A	LyA (faint continuum)
GDS J033246.05-275444.8	21.49	0.53	0.733	abs.	A	CaH, g-band, Hβ, Mg, CaFe
GDS J033246.16-274752.3	24.46	0.43	1.221	em.	B	[O II]3727

† This table is available in its entirety via `http://www.eso.org/science/goods/` and at the CDS.
A portion is shown here for guidance regarding its form and content.

For the red objects that dominate the FORS2 target selection, we felt that the improved wavelength coverage more than compensates for the possible unreliability of the flux calibration. Due to both this second order light and uncertain slit losses, we caution against using the calibrated fluxes for scientific purposes. Fluxes in the released one dimensional spectra are given in units of 10^{-16} erg s^{-1} cm^{-2} Å^{-1}.

4. Redshift determination

Spectra of 1225 individual objects have been extracted from all RUNs, out of which 887 redshifts have been determined. In the large majority of the cases the redshift has been calculated through the identification of prominent features of galaxy spectra: depending on the redshift and the nature of the source the 4000 Å break, Ca H and K, g-band, MgII 2798-2802, AlII 3584, FeII 2344, 2383 Å, Lyα, Si II 1260.4 Å, O I 1302.2 Å, C II 1335.1 Å, Si IV 1393.8, 1402.8 Å, Si II 1526.7 Å, C IV 1548.2, 1550.8 Å in absorption and Lyα, NIV]1485 Å, [O II]3727, [O III]5007, Hβ, Hα in emission. The redshift estimation has been performed cross-correlating the observed spectrum with templates of different spectral types (S0, Sa, Sb, Sc, Elliptical, Lyman Break, etc.), using the *rvsao* package in the IRAF environment. During the FORS2 campaign we have accumulated spectra of different categories (LBGs with absorption and emission lines, galaxies in the redshift interval 1.4–2, etc.) that have been used to build empirical spectral templates to identify similar spectral features in the cross-correlating process.

The redshift identifications are summarized in Table 1 and are available at the URL `http://www.eso.org/science/goods/`.

In Table 1, the column ID contains the target identifier, that is constructed out of the target position (e.g., GDS J033206.44-274728.8) where GDS stands for GOODS South. The coordinates are based on the GOODS v1.1 astrometry. The columns z_{850} and $(i_{775} - z_{850})$ list the magnitude (SExtractor "MAG_AUTO") and the color (SExtractor "MAG_ISO") of the sources derived from the catalog v1.1. The color has been measured through isophotal apertures defined in the z_{850} band image (as done in Dickinson et al. 2004; Giavalisco et al. 2004b).

The *quality* flag (QF hereafter), indicates the reliability of the redshift determination. As described in the previous works (V05, V06), the QF has been divided into three categories: "A", "B" and "C" (secure, probable and tentative redshift determination, respectively). In general the QF correlates with the goodness of the spectrum. In some cases, the presence of defects in the CCD or particularly difficult extractions may lead to very noisy one-dimensional spectrum, however, the presence of evident spectral features in the two-dimensional spectrum may still give a reliable redshift estimation. In the FORS2 campaign, 514 sources have been classified with quality "A", 226 with quality "B", 146 with "C", and 349 with "X", an inconclusive redshift spectrum.

Table 2. Journal of the entire FORS2 observations (RUN1, 2, 3, 4).

Mask ID	Date	exp.time (s)
*RUN*1 (V05)		
990247	Dec. 2002–Jan. 2003	12×1200
984829	Dec. 2002–Jan. 2003	12×1200
985831	Jan.–Feb. 2003	$15 \times 1200 + 663$
973934	Jan. 2003	12×1200
952426	Jan. 2003	12×1200
981451	Jan.–Dec. 2003	24×1200
995131	Oct. 2002	8×1800
994852	Oct. 2002	8×1800
990652	Dec.–Nov. 2002	$14 \times 1200 + 300 + 900$
*RUN*2 (V06)		
914250	Aug. 2003	17×1200
905513	Sept. 2003	18×1200
943018	Sept. 2003	12×1200
924345	Sept. 2003	12×1200
945143	Sept.–Oct. 2003	$12 \times 1200 + 3 \times 1000$
992438	Oct.–Dec. 2003	12×1200
985931	Nov. 2003	$12 \times 1200 + 2 \times 120$
990204	Dec. 2003	12×1200
904509	Dec. 2003	12×1200
991435	Dec. 2003	12×1200
935030	Dec. 2003	12×1200
951937	Dec. 2003	$12 \times 1200 + 1100 + 500$
960930	Dec. 2003	12×1200
961839	Jan. 2004	12×1200
932802	Jan. 2004	12×1200
993304	Jan. 2004	12×1200
951526	Feb. 2004	3×1200
*RUN*3		
912940	Dec. 2004	18×1200
925109	Dec. 2004	16×1200
932249	Dec. 2004	18×1200
940129	Dec. 2004	17×1200
943544	Dec. 2004	15×1200
965910	Dec. 2004	18×1200
*RUN*4		
952801	Nov.–Dec. 2005	$15 \times 900 + 4 \times 870$
952942	Oct.–Nov. 2005	$15 \times 900 + 2 \times 870$
953015	Nov. 2005	$18 \times 900 + 2 \times 870$
953048	Dec. 2005–Jan. 2006	$33 \times 900 + 2 \times 870$
953132	Feb.–Aug. 2006	$17 \times 900 + 4 \times 870 + 370$
953159	Jul.–Oct. 2006	$18 \times 900 + 2 \times 870 + 436$

The flag "*class*" groups the objects for which emission line(s) ("em."), absorption-line(s) ("abs.") or both ("comp.") are detected in the spectrum. 19 out of 887 sources have been classified as stars.

In 28% of the cases the redshift is based on single emission line, usually identified as [O II]3727 or Lyα. In these cases the continuum shape, the presence of breaks, the absence of other spectral features in the observed spectral range and the broad band photometry are particularly important in the evaluation. The quality for these sources ranges from "A" to "C"

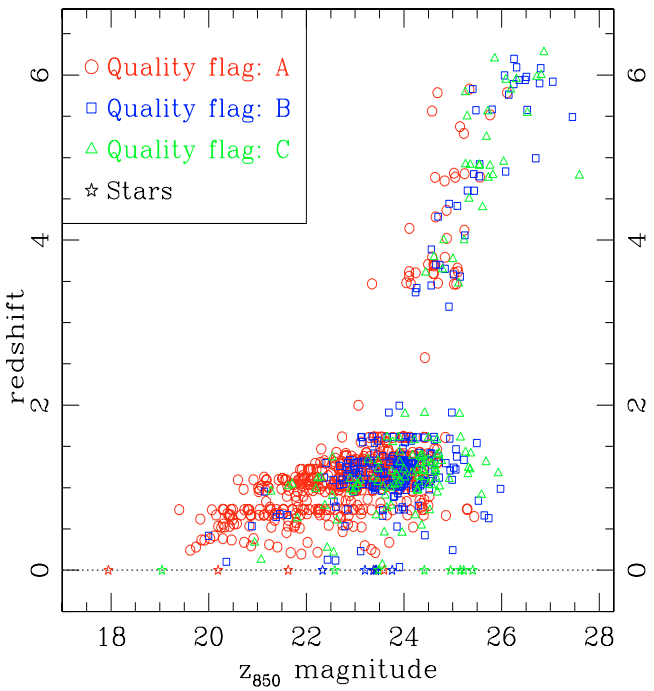

Fig. 1. Spectroscopic redshift versus magnitude for the FORS2 catalog (quality flag "A", "B", "C"). Stars are denoted by star-like symbols at zero redshift. The gap in the redshift interval $2 < z < 3.5$ is due to the spectral coverage adopted (~5800 Å–10 000 Å) and will be (partly) filled with the VIMOS spectroscopic observations.

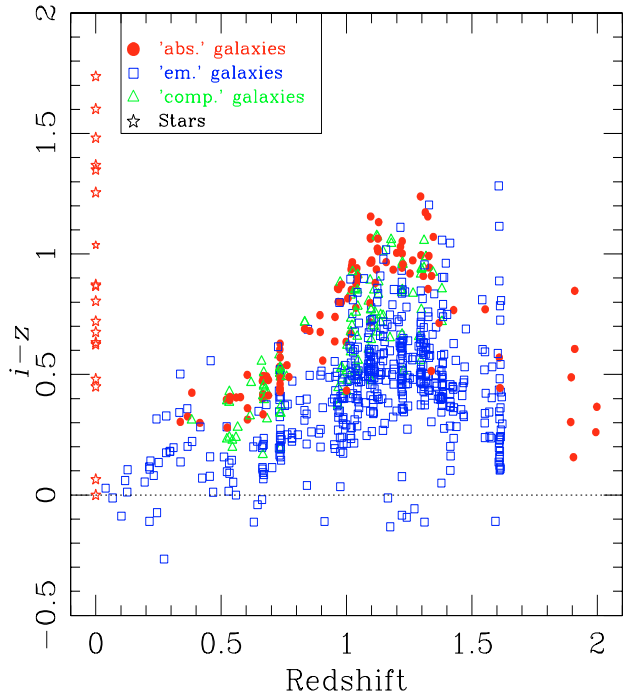

Fig. 2. Color-redshift diagram of the spectroscopic sample. Open red circles are objects identified with absorption features only ("abs." sources), while open blue squares are objects showing only emission lines ("em." sources). The intermediate cases are shown by open green triangles ("comp." sources).

depending on the additional information described above (30% of the sample with a single emission line have QF = "A").

The *comments* column contains additional information relevant to the particular observation. The most common ones summarize the identification of the principal lines, the inclination of an emission line due to internal kinematics, the weakness of the signal ("faint"), the low S/N of the extracted spectrum ("noisy"), the apparent absence of spectroscopic lines ("featureless continuum"), etc.

In few cases the spectrum extracted is the combination of more than one source in the slit and where possible the redshifts of the "components" have been estimated separately. In all FORS2 sample, 11 sources in the GOODS-S field are not present in the ACS photometric catalog v1.1. Six of them have a redshift estimation. Three out of six appear to be emission line objects whose continuum is too faint and has not been detected in the z_{850} band. The other seven sources are outside the GOODS-S area.

4.1. Reliability of the redshifts – diagnostic diagrams

Figures 1 and 2 show the redshift-magnitude and the color-redshift distributions, respectively.

From Fig. 1 it is evident that the number of low quality redshift measurements increase with increasing magnitude. Also in the case of low redshift galaxies $z < 0.5$ the uncertainty increase due to the adopted spectral range (~6000 up to ~10 000 Å). In other few cases, serendipitous relatively bright sources enter in the slit because of the dithering shift, for those sources the exposure time is reduced and the sky subtraction complicated. In these cases the quality of the reduced spectra tends to be lower.

Figure 2 shows the behavior of the color-redshift for galaxies at redshift less than 2, where the two populations of "emission-line" (star-forming) and "absorption-line" (typically elliptical) galaxies are clearly separated. As expected, the mean color of the absorption-line objects outline the upper envelop of the distribution. The intermediate cases "comp." with emission and absorption features (green triangles) lie in the middle. The presence of LSS in the field (and discussed below) is evident in the figure as vertical concentrations of points at redshifts ~0.7, 1.1, 1.2, 1.3, 1.6.

The emission-line objects show in general a bluer $i_{775} - z_{850}$ color and a broader distribution than the absorption-line sources. Such bimodality in the color distribution with a larger scatter of the blue component with respect to the red one has been observed in other surveys and can be ascribed to the different star formation histories (SFHs) of the two populations. The former being the result of a large variety of SFHs that extend to much lower redshift than the red ones (resulting in their scattered bluer colors), the latter the result of a more similar SFHs in which the bulk of the activity happens at higher redshift (Menci et al. 2005).

5. Discussion

The present release lists 1225 spectra. 887 out of 1225 sources have a redshift determination (19 are stars, $z = 0$), corresponding to a success rate on the redshift determination of about 72% (assuming that all redshift measurements are correct). Sources with inconclusive redshift measurement are in general faint or without reliable spectral features (indicated in the "comment" column as *featureless continuum* or *faint continuum*). The observations aimed at a uniform sky coverage of the GOODS-S field.

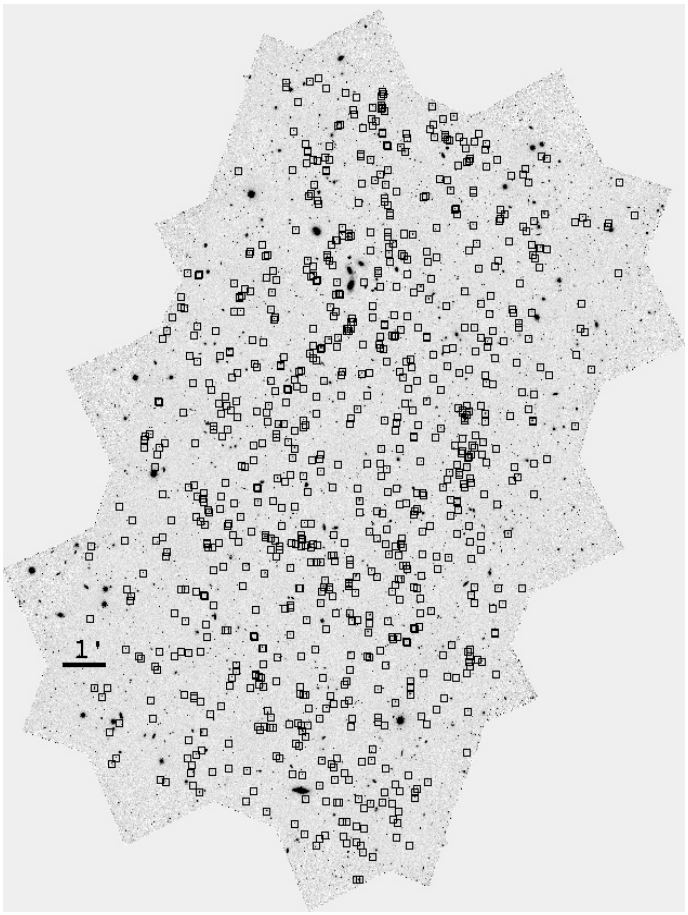

Fig. 3. Spatial distribution in the GOODS-S field of the FORS2 spectroscopic catalog (887 redshift determinations).

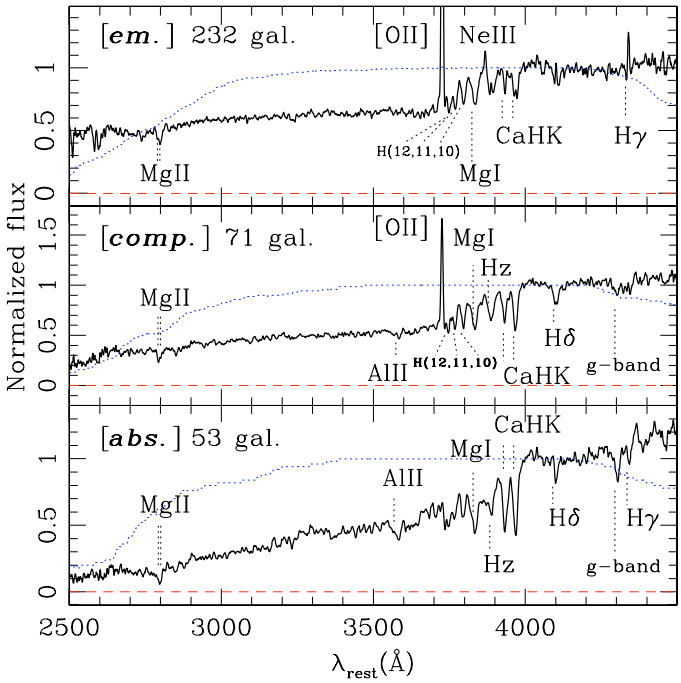

Fig. 4. Composite spectra of the three categories "em.", "comp." and "abs." from top to bottom, respectively (QF = "C" has not been considered). The median redshift for all is $z \sim 1$. The co-addition has been weighted and the final spectrum normalized to unity in the wavelength range 4000–4100 Å. In the top panel, the [O II]3727 line is not fully shown. The weight-function is shown as dotted blue line and have also been normalized to unity (1 means that all spectra contribute to the sum, 0.5, half of them, etc.).

Table 3. Number of sources in the redshift interval $3 < z < 6.3$ with different spectral features.

Redshift range	A	B	C	N
$3 < z \leq 4.5$	26	14	11	51
$4.5 < z \leq 5.5$	8	9	14	31
$5.5 < z \leq 6.5$	5	17	10	32
N	39	40	35	114

Table 4. Number of sources in the redshift interval $0 < z < 2$ with different spectral features (without stars).

Class	$z_{\rm median}$	$z_{\rm min}$	$z_{\rm max}$	A	B	C	N
emission	1.140	0.039	1.621	282	152	84	518
absorption	1.005	0.337	1.998	86	18	21	125
em. and abs.	1.022	0.382	1.380	101	9	0	110
Total	1.098	0.039	1.998	469	179	105	753

Six FORS2 MXU-masks are necessary to cover the 150 square arcmin of the GOODS-S field, so with 38 masks (the entire FORS2 campaign) the field has been covered roughly ∼6 times (the spatial distribution of the 887 sources in the GOODS-S area is shown in Fig. 3).

114 targets out of 887 are confirmed to be LBGs in the redshift range $3 < z < 6.3$ (see Table 3), in agreement with the dropout selection techniques (Giavalisco et al. 2004b; Dickinson et al. 2003).

753 out of 772 sources at redshift less than 2 have been identified as galaxies (19 are stars, see Table 4). 628 of them (including "em." and "comp" classes) show the [O II]3727 emission up to redshift 1.621, while 125 galaxies identified with absorption lines only ("abs." class, mainly Ca H and K, MgII 2798–2802) span the range of redshift between 0.3–2.0. The composite spectra of the three categories "em." (232 star-forming galaxies), "comp" (71 intermediate galaxies) and "abs." (53 elliptical galaxies) selected in the redshift range 0.8–1.3 are shown in Fig. 4, from top to bottom panels, respectively.

Hδ and g-band are not detected in the "em."-like galaxies, but they are well detected in the other two categories, consistently with the presence of older stellar populations. Lines of the Balmer series have been detected down to H12. All composite spectra show MgII in absorption.

Obviously, in the presence of emission lines, it is easier to determine a redshift. As an extreme example, emission lines may be identified without the presence of the continuum in the spectrum (if the equivalent width is sufficiently large), while absorption lines not. For this reason the detection of absorption features in relatively faint sources is more uncertain and more sensitive to the residuals in the sky subtraction, on average they are one magnitude brighter than the emission lines galaxies (the average z_{850} magnitude of "em."-like galaxies is 23.65 with redshift measurements up to $z_{850} = 26$, while "abs."-like galaxies have an average of 22.44 and with redshift measurements up to $z_{850} = 25$). A flavour of this effect is shown in Fig. 5, where the coverage of the [O II]3727 line (top panel) and Ca H and K absorption doublet (bottom panel) over the sky emission spectrum is shown as a function of the measured redshift. We note that the [O II]3727 emission has been detected even over the peaks of the strongest sky emission lines, while the absorption features tend

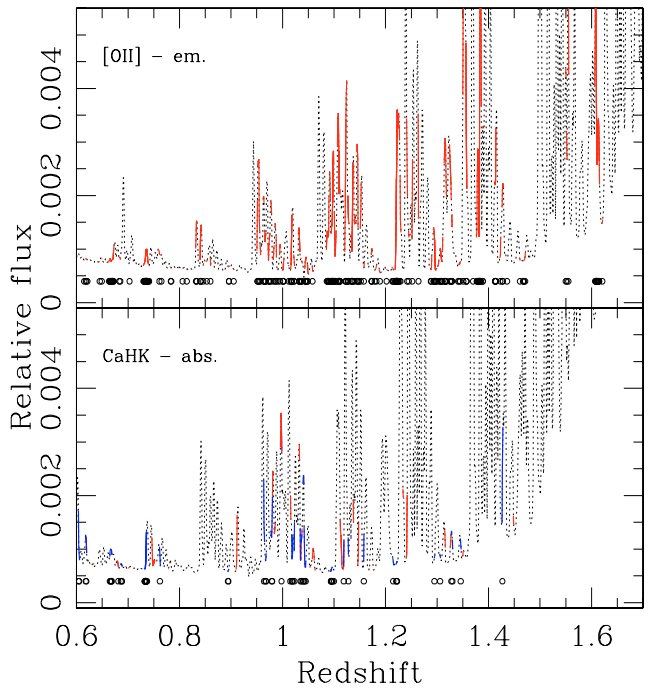

Fig. 5. Coverage in the sky emission spectrum by the principal lines used in the redshift determination, [O II]3727 for emitters (*top panel*) and Ca H and K for ellipticals (*bottom panel*, blue K3933.7 Å and red H3968.5 Å). Black open circles denote the redshift position in the spectrum.

to be identified in the valleys between the sky lines, in particular beyond redshift 1 (e.g. ellipticals detected at redshift $z \sim 1.3$).

This is a likely reason why the majority of galaxies identified in the present work belong to the "em." class. Alternatively, or in addition to observational effects, the [O II]3727 is a classic star forming indicator and the redshift interval $1 < z < 2$ corresponds to the peak of the mean star formation intensity of the universe.

5.1. Completeness of the sample

A direct way to derive a rough estimate of the completeness of the present sample is to compare spectroscopic and photometric redshifts down to a common magnitude limit and bins of redshift. We have used the recent photometric redshift measurements in the GOODS-S field, based on the "PSF-matched" GOODS-MUSIC photometric catalog of Grazian et al. (2006). As shown in that work, photometric redshifts have been estimated with great accuracy, reaching an average scatter of $\sigma = 0.06$. Table 5 summarize the completeness of the spectroscopic sample described in the present work. Column two shows the number of spectroscopic redshifts and columns three, four and five show the spectroscopic completeness in each redshift bin (Nzspec/Nzphot) down to $z_{850} = 24$, 25 and 26, respectively. As targeted, part of the FORS2 campaign has identified galaxies mainly in the redshift range 0.8–2 (see also Fig. 6, middle and bottom panels). At present, at redshift ∼1.2 the completeness is ∼30% down to $z_{850} = 26$.

In the top panel of Fig. 6 the photometric redshift distribution of galaxies in the GOODS-S field with redshift less than 2 and magnitude z_{850} brighter than 26 is shown. The spectroscopic redshift distribution is shown in the bottom panel of the same figure, with a magnitude limit $z_{850} \sim 26$. One of the main target of the FORS2 campaign is to provide spectroscopic

Table 5. Completeness of the entire spectroscopic sample describe in the present work down to $z_{850} = 26$.

z bin	zspec	compl.(%) $z_{850} < 24$	compl.(%) $z_{850} < 25$	compl.(%) $z_{850} < 26$
[0.6..0.7[	46	11	7	5
[0.7..0.8[	62	26	18	13
[0.8..0.9[	23	17	9	5
[0.9..1.0[	54	22	11	7
[1.0..1.1[	130	48	29	20
[1.1..1.2[	85	77	44	27
[1.2..1.3[	107	84	45	30
[1.3..1.4[	86	67	31	19
[1.4..1.5[	30	48	19	10
[1.5..1.6[	15	37	11	6
[1.6..1.7[	33	84	32	18
[1.7..1.8[	0	0	0	0
[1.8..1.9[	2	12	3	1
[1.9..2.0[	5	36	8	3
[2.0..2.1[	0	0	0	0

identifications in the redshift range 0.8–2, according to the color selection criterium $(i - z) > 0.45$ (or $(i - z) > 0.6$ for the redder ones, see Sect. 2). The photometric redshift distribution down to $z_{850} = 26$ of sources with $(i - z) > 0.45$ is shown in the middle panel of Fig. 6, in which it is evident that the color cut selects mainly galaxies at redshift beyond 1. Apart from the normalization, the two distributions (middle and bottom panels) show a similar shape. Both the photometric and spectroscopic redshift distributions of sources with $(i - z) > 0.45$ show approximately 90% of galaxies at redshift beyond 0.8. The percentage increases to 96% if we restrict the color cut to $(i - z) > 0.6$. As discussed in V06 and recalled in Sect. 2, galaxies in the redshift interval 0.8–2 were selected also on the basis of photometric redshifts provided by Mobasher et al. (2004), for this reason the present sample contains confirmed galaxies at redshift beyond 1 and bluer than $(i - z) = 0.45$ (see also Fig. 2).

5.2. Redshift distribution and large scale structure

The top and bottom panels of Fig. 7 show the redshift distribution of the galaxies at redshift less than 2 and greater than 3, respectively (solid line QF "A" and "B", dotted line QF "C"). Galaxies have been counted in a variable bin dz which has been moved across the redshift interval with a step of 0.003 (of the order of 3 times the error of the redshift estimation). The bin dz has been calculated at each redshift to be equivalent to a velocity dv = 2000 km s^{-1}, so the binning in Fig. 7 is constant in the velocity space (d$z = (1 + z) \times$ dv/c where c is the speed of light).

In general, the redshift distribution is consistent with the selection criteria adopted, with the majority of the sources having redshifts in the interval $1 < z < 2$ and $z > 3$ (top and bottom panels of Fig. 7, respectively).

At redshift less than 2, as discussed in the previous work (V06) and including the new spectroscopic identifications (RUN3 and 4), large scale structures are confirmed by the spikes at redshift 0.667 (23 galaxies), 0.735 (49 galaxies), 1.096 (43 galaxies), 1.220 (53 galaxies), 1.301 (40 galaxies), 1.382 (28 galaxies) and 1.611 (32 galaxies). Some of these peaks are already know in literature (Cimatti et al. 2002; Gilli et al. 2003; Le Fevre et al. 2004; Adami et al. 2005; Cimatti et al. 2004). The overdensity of galaxies detected at $z \sim 1.61$ is increased by 50% from the

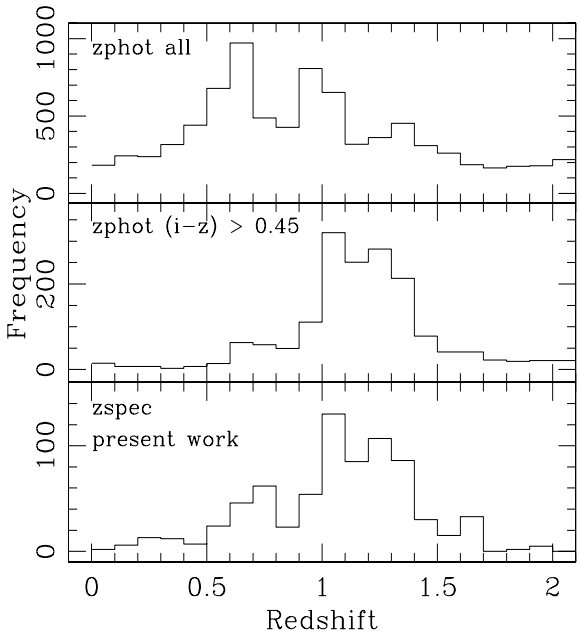

Fig. 6. Completeness of the FORS2 spectroscopic sample at redshift less than 2. In *the upper panel* the photometric redshift (*z*phot) distribution down $z_{850} = 26$ is shown. In the *middle panel*, the *z*phot distribution has been plotted adding the main color selection criterium adopted in the FORS2 spectroscopic campaign ($(i - z) > 0.45$, see Sect. 2). In *the bottom panel* the spectroscopic redshift distribution of the present work is shown. The values of the completeness are shown in Table 5. Photometric redshifts have been drawn from Grazian et al. (2006).

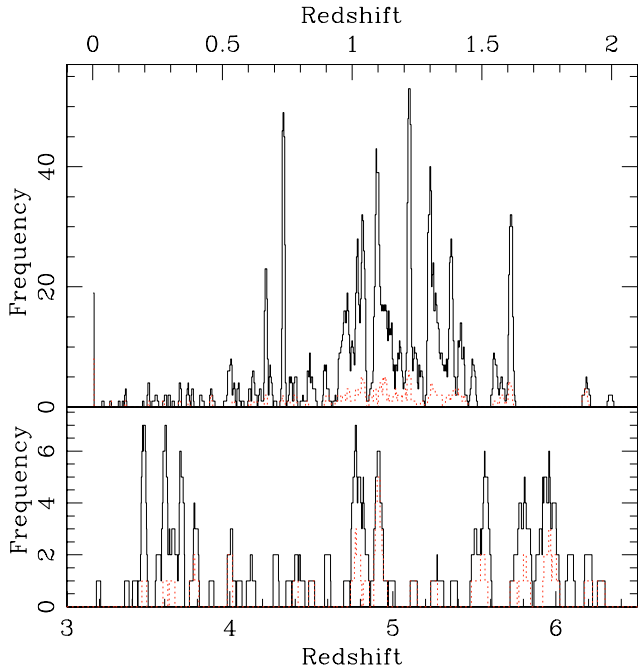

Fig. 7. Redshift distribution according to the selection functions described in Sect. 2 for the spectroscopic sample with quality A, B (solid line) and C (dotted line). In the top and bottom panels the sources at $z < 2.1$ and $z > 3$ are shown, respectively. The redshift bin is calculated at each redshift and corresponds to a velocity interval $dv = 2000$ km s^{-1}.

previous releases, and counts more than 30 galaxies, all identified through the [O II]3727 emission at ~9730 Å.

Comparing the roughly expected (photometric)redshift distribution in GOODS-S field (middle panel of Fig. 6) and the observed one, we note (see Fig. 7) possible underdensities of galaxies in the redshift interval 1–1.5, particularly at 1.06–1.08 and 1.27–1.28. The former is close to the sky "A"-band absorption where the transmission is approximately less that 50% and acts mainly in the [O II]3727 redshift interval 1.03–1.06 (with a less absorbing tail up to 1.074, `http://tdc-www.harvard.edu/instruments/hectospec/habsky.html`). This sky absorption band is not introducing an evident bias, 42 [O II]3727 emission line galaxies have been identified in the more sky absorbed redshift range 1.03–1.06, only 3 galaxies in the redshift interval 1.06–1.08 (zero sources between 1.06–1.07) and 47 galaxies in the range 1.08–1.10 where there is the overdensity discussed above.

At redshift beyond 3, galaxies show the expected mean redshift consistently with the color selection criteria (Giavalisco et al. 2004b; Dickinson et al. 2004). B_{435}, V_{606} and i_{775}-dropouts sources have been confirmed to be at $\langle z \rangle = 3.7$, 4.9 and 5.9, respectively. The success rate of the spectroscopic redshift measure for these categories is of the order of 70% and the efficiency of the selection is greater than 80% (Vanzella et al., in preparation).

6. Individual notes

6.1. A double peaked Lyα emission line at redshift 3.7

The source GDS J033217.22-274754.4 has been selected as B_{435}-dropout galaxy and has been confirmed to be at redshift 3.649. The main spectral feature is the Lyα emission line and the break of the continuum just blueward the line. Two interstellar absorption lines (SiII 1526.7 and CIV 1548.2,1550.8) have also been detected (see Fig. 8).

The emission line at wavelength ~5650 Å shows an evident double peaked structure (see Figs. 8 and 9) with a separation of ~13 Å.

Several authors have analyzed the transfer of Lyα photons in static and expanding neutral clouds in various physical conditions (Adams 1972; Urbaniak & Wolfe 1981; Zheng & Miralda -Escudè 2002; Ahn et al. 2003; Verhamme et al. 2006). If the shell is static, the profile shows two emission peaks with the same flux, blueshifted and redshifted with respect the systemic redshift. In the present case the two peaks show different intensities and the observed separation is much larger than the expected separation produced by a static shell (0.24 Å at the redshift of the galaxy), hence, the outflow of material seems to be the most plausible reason.

In the outflow picture, the flux of the blue peak is decreased if the expansion velocity of the shell is increased and also its position depends to the velocity expansion. Powered by star formation and supernova explosions, a wind creates a large shell of swept up material and the observation towards such an object would intersect the shell in the front and the rear end giving rise to a double peaked emission line profile. If the expansion velocity is sufficiently high, the blueshifted secondary peak disappears and the red wing of the Lyα profile get more flux producing the characteristic asymmetric profile observed in high redshift star forming galaxies. Such double peaked profiles of optical emission lines have been observed for nearby starburst galaxies which exhibit these large scale outflows typically termed superwinds (Heckman et al. 1990). Additionally, a double peaked Lyα emission line profile

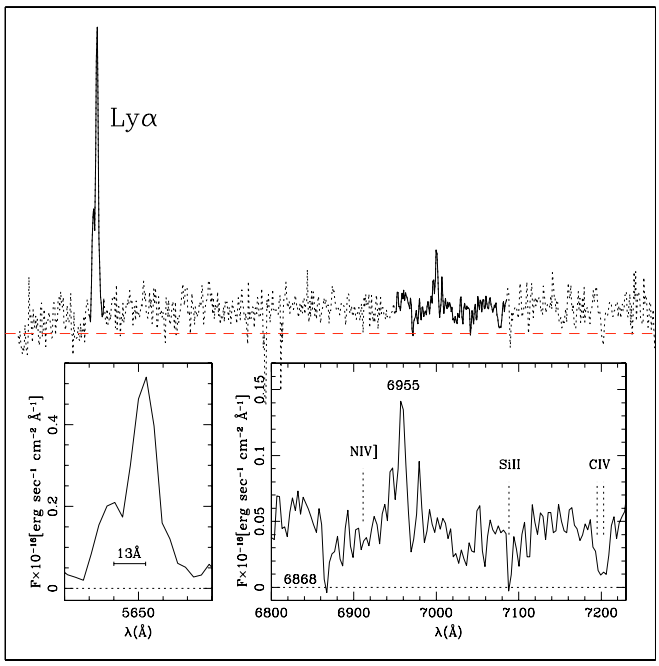

Fig. 8. One dimensional spectrum of the B_{435}-dropout galaxy GDS J033217.22-274754.4. The bottom panel zoom the solid line regions of the spectrum marked above. The double peaked Lyα line is evident with a separation between peaks of ∼13 Å. SiII 1526.7 and CIV 1548.2,1550.8 have been detected at redshift consistent with Lyα. Other two spectral features have been detected at 6868 and 6955 Å.

was found from the starburst galaxy T1214–277 by Mas-Hesse et al. (2003), who concluded that the feature is caused by emission in an outflow. Double-peaked Lyα profiles have been observed also at redshift $z \sim 3$, in spectra of star forming galaxies (Fosbury et al. 2003; Christensen et al. 2004; Venemans et al. 2005; Tapken et al. 2007).

In the present case, the measured separation between the two peaks (13 Å) is probably due to an expanding neutral cloud. Moreover, it is worth to note that the redshift of the blue peak is consistent with the redshift derived from the SiII 1526.7 and CIV 1548.2,1550.8 lines (see Table 6). This indicates a plausible connection between the outflow of the gas deduced from the double peaked Lyα profile and that observed from the interstellar lines: the blue peak of the Lyα line and the interstellar absorption lines are possibly probing the same behavior of the medium (material approaching the observer). Interpreting the double-peak as due to an expanding shell, the velocity difference between the two peaks corresponds to $2 \times V\mathrm{exp}$ (Verhamme et al. 2006). The inferred velocity $V\mathrm{exp}$ (∼320 km s^{-1}) is consistent with the value measured by Shapley et al. (2003) from the velocity difference between stellar and interstellar lines in a large sample of LBG spectra at redshift ∼3.

It is worth to note that other two lines have been detected on the spectrum, one in absorption (6868 Å) and the other in emission (6955 Å), that have not been identified. Detailed spectroscopic observations have to be performed in order to clarify the nature of such "additional" lines.

6.2. MgII absorbers at z = 1.61 in spectra of LBGs at z > 3?

Two galaxies, GDS J033226.18-275211.3 and GDS J033226.76-275225.9 selected as U and B_{435}-dropout, respectively, have been observed during the FORS2 and VIMOS campaign (Popesso et al. in preparation).

Table 6. Lines identified in the spectrum of B_{435}-dropouts GDS J033217.22–274754.4.

Line	λ(Å)	Redshift
	emission	
Lyα(1215.8) (blue)	5647	3.645
Lyα(1215.8) (red)	5660	3.655
??	6955	
	absorption	
??	6868	
SiII(1526.7)	7089	3.643
CIV(1548.2-1550.8)	7200	3.647

In the case of GDS J033226.76-275225.9 (bottom panel of Fig. 10) the measured redshifts from FORS2 (3.562, QF = "A") and VIMOS (3.554, QF = "C") agree within the errors. In the FORS2 spectrum, the CII 1335.1, SiII 1526.7 and CIV 1548.2,1550.8 have been detected. The latter doublet shows a *FWHM* larger than other single lines (see Fig. 10 where the numbers in the parenthesis indicate the *FWHM* of the lines). The absorption line at 7331.1 Å may be associated to FeII 1608.5 in absorption at the redshift of the galaxy. However such a feature is unusual if compared with other LBGs, moreover the *FWHM* of the line is evidently large (37 Å) with respect to the other lines.

Similarly, in the spectrum of GDS J033226.18-275211.3 there is an absorption line with a *FWHM* that apparently is not consistent with the redshift of the source ($z = 3.057$ from the VIMOS spectroscopic survey). The redshift is not reliable (QF = "C") and the FORS2 absorption features (marked with their *FWHM* in the top panel of Fig. 10) are not consistent with the VIMOS redshift. However, the two relatively strong absorption lines around 7300 Å seem to have no easy solution if associated to the galaxy. We note that also in this case the line at 7349.0 Å shows a *FWHM* of 34.1 Å, similarly to the line discussed above.

The fact that the two galaxies are relatively close in the sky (16.5 arcsec) and show two features at similar wavelength, apparently not consistent with the galaxy redshift, support the interpretation in terms of intervening absoprtion. Moreover, in both cases, the *FWHM* of the lines is large and suggest the presence of a doublet (as we see for the CIV 1548.2,1550.8 doublet, bottom panel of Fig. 10). Interestingly, if the two spectral features are MgII 2798,2802 absorbers, their redshifts turns out to be 1.618 and 1.624, very close to the overdensity at redshift 1.611 detected in the field (see Fig. 7 and Sect. 5.2).

Unfortunately no confirmed galaxy at redshift 1.61 has been currently identified in the neighborhood of the high-z ones (the closest one is at a physical separation of ∼900 kpcs from them), further spectroscopic investigations would be necessary to shed light on the nature of the absorbers. The physical separation of the absorbers (140 kpcs) and possible candidate members of the overdensity at $z = 1.61$ associated with the present MgII features are shown in Fig. 11 (triangles indicate sources with photometric redshift in the interval 1.4–1.8).

7. Conclusions

As a part of the Great Observatories Origins Deep Survey, a large sample of galaxies in the Chandra Deep Field South has been spectroscopically targeted. After the RUN1 (V05),

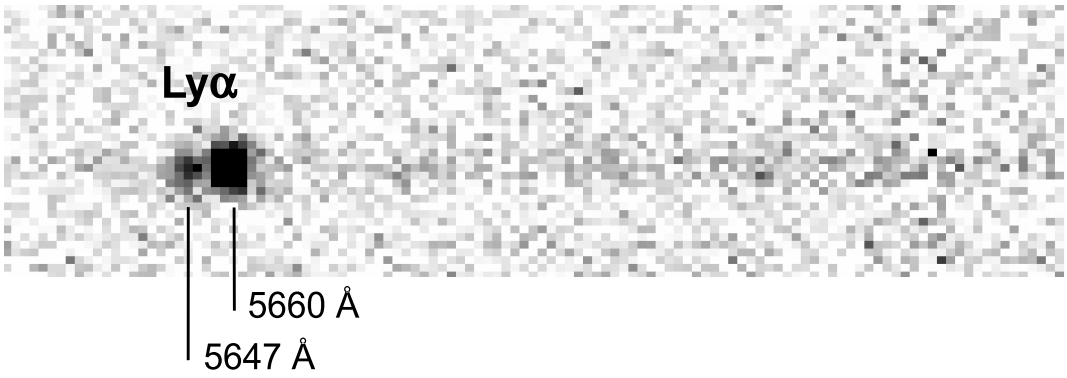

Fig. 9. Two dimensional spectrum of the B_{435}-dropout galaxy GDS J033217.22-274754.4, the wavelength range 5590–5950 Å is considered. The double peaked line is evident with the continuum redward the structure. The blue spot and the more intense red one are separated by 13 Å and are aligned with the continuum of the target. If one of the two lines is a contamination of the close source GDS J033217.24-274753.4 at 0.9 arcsec separation from the target, an offset would be expected in the spatial direction. During the observations of this galaxy the average seeing was ~0.7 arcsec.

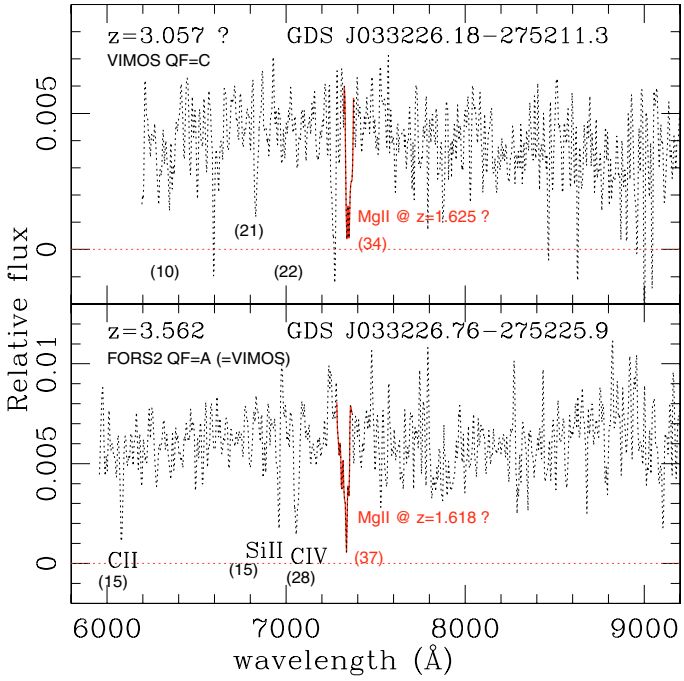

Fig. 10. One dimensional spectra of two galaxies at redshift 3.057 (*top panel*) and 3.562 (*bottom panel*). In the bottom case the redshift estimation is reliable (FORS2 agree with the VIMOS one). The top source has a VIMOS redshift 3.057 with quality "C", but no evident correspondence has been found with the absorption feature detected in the FORS2 spectrum. Both spectra show an absorption line at 7349.6 Å (*top*) 7331.9 Å (*bottom*), apparently not consistent with the redshift of the host galaxy. The *FWHM* of the lines is shown within parenthesis. If interpreted as MgII foreground absorbers (the *FWHM* of the lines suggest a doublet), they would be at redshift 1.61, at the same redshift of the overdensity discussed above. The physical separation at $z \sim 1.61$ between them is 140 kpcs.

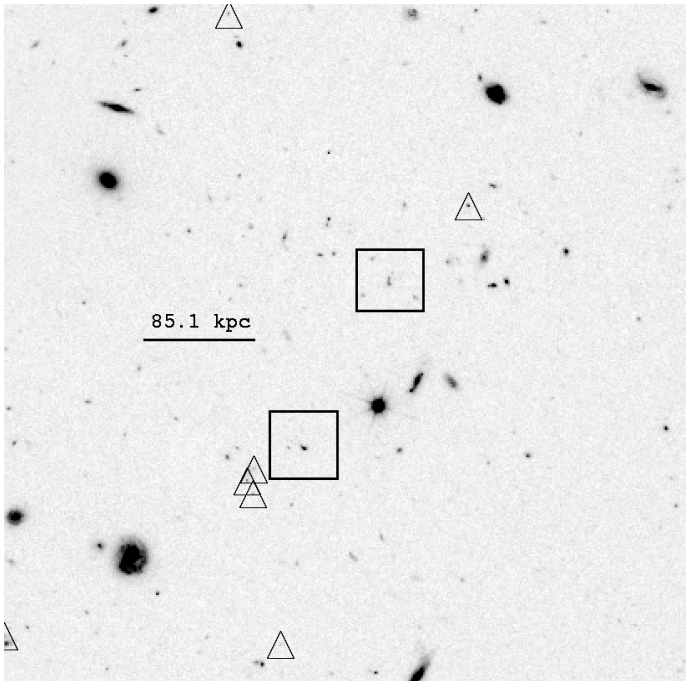

Fig. 11. z850 ACS image of a portion of the GOODS-S field. The two galaxies at redshift beyond 3 which display possible MgII in absorption at $z \sim 1.61$ are marked with squares. The physical separation between them at $z = 1.61$ is ~140 kpc (10 arcsec correspond to 85.1 kpc, segment in the figure). Sources with photometric redshift in the interval 1.4–1.8 are marked with triangles. The image is one square arcminute size.

RUN2 (V06) and the present work (RUN1, 2, 3, 4) a total of 1225 objects with $z_{850} \lesssim 27$ have been observed with the FORS2 spectrograph at the ESO VLT providing 887 redshift determinations with a typical $\sigma_z \simeq 0.001$ (16% of the sample has a tentative redshift measurement, QF = "C"). The reduced spectra and the derived redshifts are released to the community (`http://www.eso.org/science/goods/`). They constitute an essential contribution to reach the scientific goals of GOODS, providing the time coordinate needed to delineate the evolution of galaxy masses, morphologies, and star formation, calibrating the photometric redshifts that can be derived from the imaging data at 0.36–8 μm and enabling detailed studies of the physical diagnostics for galaxies in the GOODS field.

Two individual sources have been discussed: 1) a double peaked Lyα profile at redshift ~3.7 due to outflow of material powered by star formation and supernova explosions and 2) the possible detection of two (relatively close, 16.5 arcsec) MgII absorbers at redshift 1.61 (the same of the overdensity already confirmed in the field) observed through spectra of LBGs.

Acknowledgements. We are grateful to the ESO staff in Paranal and Garching who greatly helped in the development of this programme. We wish to thank the referee for comments which improved the paper.

References

Adami, C., Mazure, A., Ilbert, O., Cappi, A., & the VIMOS VLT Deep Survey team 2005, A&A, 443, 805
Adams, T. F. 1972, ApJ, 174, 439
Ahn, S. H., Lee, H. W., & Lee, H. M. 2003, MNRAS, 340, 863
Alonso, M., Sol, L., Diego, G., Tissera, P., & Coldwell, G. 2007, MNRAS, 375, 1017
Bunker, A. J., Stanway, E. R., Ellis, R. S., & McMahon, R. G. 2003, MNRAS, 324, 47
Christensen, L., Sanchez, S. F., Jahnke, K., et al. 2004, A&A, 487, 498
Cimatti, A., Mignoli, M., Daddi, E., et al. 2002, A&A, 392, 395
Cimatti, A., Daddi, E., Renzini, A., et al. 2004, Nature, 430, 184
Cristiani, S., Appenzeller, I., Arnouts, S., et al. 2000, A&A, 359, 489
Croom, Scott, M., Warren, S. J., & Glazebrook, K. 2001, MNRAS, 328, 150
Dickinson, M., & GOODS Legacy Team 2001, AAS, 198, 250
Dickinson, M., & Giavalisco, M. 2003, in the proceedings of the ESO/USM Workshop The Mass of Galaxies at Low and High Redshift (Venice, Italy, October 2001), ed. R. Bender, & A. Renzini [arXiv:astro-ph/0204213]
Dickinson, M., Stern, D., Giavalisco, M., et al. 2004, ApJ, 600, 99
Fosbury, R. A. E., Vilar-Martin, M., Humphery, A., et al. 2003, ApJ, 596, 797
Giavalisco, M., Ferguson, H. C., Koekemoer, A. M., et al. 2004a, ApJ, 600, L93
Giavalisco, M., Dickinson, M., Ferguson, H. C., et al. 2004b, ApJ, 600, 103
Gilli, R., Cimatti, A., Daddi, E., et al. 2003, ApJ, 592, 721
Grazian, A., Fontana, A., de Santis, C., et al. 2006, A&A, 449, 951
Heckman, T. M., Armus, L. M., & George, K. 1990, ApJS, 74, 833
Le Fèvre, O., Vettolani, G., Paltani, S., et al. 2004, A&A, 428, 1043
Le Fevre, O., Vettolani, G., Garilli, B., Tresse, L., & the VIMOS VLT Deep Survey team 2005, A&A, 439, 845
Mas-Hesse, J. M., Kunth, D., Tenorio-Tagle, G., et al. 2003, ApJ, 598, 858
Menci, N., Fontana, A., Giallongo, E., & Salimbeni, S. 2005, ApJ, 632, 49
Mignoli, M., Cimatti, A., Zamorani, G., et al. 2005, A&A, 437, 883
Mobasher, B., Idzi, R., Benítez, N., et al. 2004, ApJ, 600, 167
Oke, J. B. 1977, ApJS, 27, 21
Papovich, C., Moustakas, L. A., Dickinson, M., et al. 2006, ApJ, 640, 92
Patton, D. R., Carlberg, R. G., Marzke, R. O., et al. 2000, ApJ, 536, 153
Ravikumar, C. D., Puech, M., Flores, H., et al. 2007, A&A, 465, 1099
Renzini, et al. 2002, in the proceedings of the ESO/USM Workshop The Mass of Galaxies at Low and High Redshift (Venice, Italy, October 2001), ed. R. Bender, & A. Renzini
Riess, A. G., Strolger, L.-G., Tonry, J., et al. 2004, ApJ, 607, 665
Shapley, A. E., Steidel, C. C., Pettini, M., & Adelberger, K. L. 2003, ApJ, 588, 65
Stanway, E. R., Bunker, A. J., McMahon, R. G., et al. 2004, ApJ, 607, 704
Strolger, L. G., Riess, A. G., Dahlen, T., et al. 2004, ApJ, 613, 200
Szokoly, G. P., Bergeron, J., Hasinger, G., et al. 2004, ApJS, 155, 271
Tapken, C., Appenzeller, I., Noll, S., et al. 2007, A&A, 467, 63
Vanzella, E., Cristiani, S., Dickinson, M., et al. 2005, A&A, 434, 53
Vanzella, E., Cristiani, S., Dickinson, M., et al. 2006, A&A, 454, 423
Verhamme, A., Schaerer, D., & Maselli, A. 2006, A&A, 460, 397
Venemans, B. P., Rottgering, H. J. A., & Miley, G. K. 2005, A&A, 431, 793
Warmels, R. H. 1991, The ESO-MIDAS System, in Astronomical Data Analysis Software and Systems I, PASP Conf. Ser., 25, 115
Woods, D. F., & Geller, M. J. 2007, AJ, 134, 527
Urbaniak, J. J., & Wolfe, A. M. 1981, ApJ, 244, 406
van der Wel, A., Franx, M., van Dokkum, P. G., & Rix, H.-W. 2004, ApJ, 601, 5
Zheng, Z., & Miralda-Escudè, J. 2002, ApJ, 578, 33